25th ABCM International Congress of Mechanical Engineering
October 20-25, 2019, Uberlândia, MG, Brazil.

COB2019-2286
PHYSICAL ANALYSIS AND CHARACTERIZATION OF A RAIL *SQUAT* DEFECT

Gregory de Oliveira Miranda
Vinicius Silva dos Reis
gregmirandamail@gmail.com
viniciusreis11@hotmail.com

Carlos Vinícius de Paes Santos
Carlos.paes@ifpa.edu.br

Andrey Coelho das Neves
andreycoelho143@gmail.com

Ricardo Nazareno Costa França
ricardoncf86@gmail.com

Clóvis Iarlande Oliveira Santana
Clovis.mecanica@hotmail.com

José Maria do Vale Quaresma
Universidade Federal do Pará. Rua Augusto Corrêa,1. Belém, Pará
jmquaresma@ufpa.br

Abstract. *Rails are components that have a variety of functions, such as guiding the rail vehicle and transmitting the efforts of loading the rail vehicle to the track infrastructure. Since they are subject to stresses that originated from the service (bending, vertical, thermic) and fabrication (residual), they can start defects and cause catastrophic failures. The objective of this study is to characterize one rail surface defect in a sample provided by the company VALE S/A and to define its initiation and grow, in addition to other characteristics involved. RCF cracks have been examined in detail by scanning electron and optical microscopy. Microhardness tests were performed, and the rail microstructure has been evaluated. The results proved that it was a typical squat defect, also known as dark spot originated from surface-initiated cracks. The microhardness results presented the typically expected profile, with larger values on the surface and decreasing with the depth.*

Keywords: ***Rail defect, rolling contact fatigue, wheel-rail contact***

1. INTRODUCTION

Rails are structures susceptible to failure because they are subject to various loads and external influences such as high stresses, mechanical wear, climatic variations, and others (Cannon et al., 2003). By failure is meant the wear, the defects, in the last case, the fracture. One family of rail defects that have motivated international research in recent decades is the rolling contact fatigue damage (RCF). These defects mainly manifest in the form of cracks in the rail surface. The most common types of RCF are head check, which in some cases occurs on external curve rails and may have its genesis from sub-superficial ratcheting defect (Grassie and Kalousek, 1977), and squats on rail running surface.

When the stresses from the loading exceed the material flow limit of the wheels and rails, each loading cycle causes cumulative plastic deformation, causing an alignment of the eutectoid lamellas, which may cause dissociation (Fig.1). With increasing deformation, small fatigue cracks can start in the contact region (Franklin et al., 2008) and under certain conditions they can propagate internally to the rail and cause it to break (Huang et al., 2018).

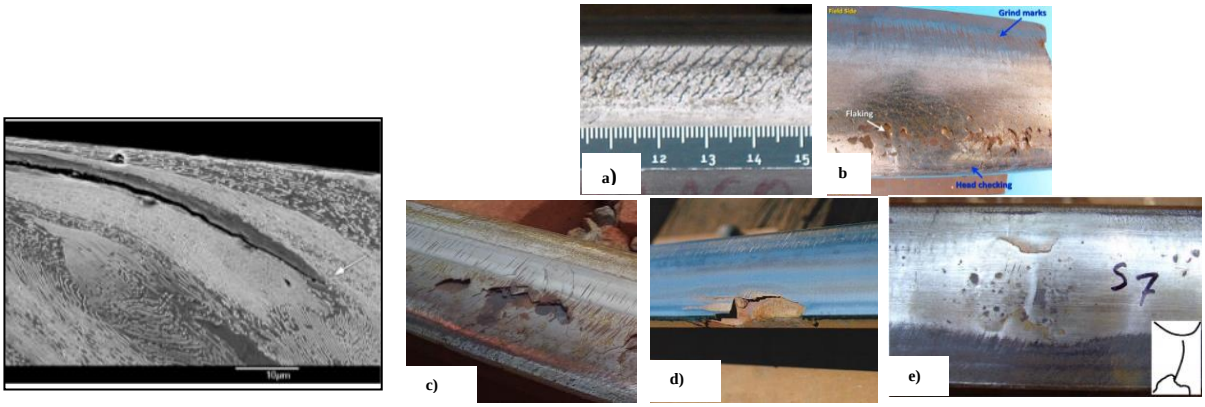

Figure 1. RCF crack propagation, following the sheared, dissociated, and aligned euthetoid microstructure. This deformation is known as ratcheting. Source: Garnham and Davis, 2011. Main RCF rail defects types: (a) Head Check. Source: Popović et al., 2015, (b) Flaking. Source: Zakar and Mueller, 2016, (c) Spalling. Source: From the survey, (d) Shelling. Source: Handbook Rail Track, 2006, and (e) Squat. Source: Li, 2011.

Fig.1a illustrates the head check that is characterized by shallow cracks that are usually visible in the corner gauge regions. Besides, another defect that may originate from this is flaking, shown in Fig.1b. This defect manifests itself as a slight removal of material from the rail surface. Also, Fig.1c shows the spalling, which is characterized as the most severe removal of material from the rail running surface and gauge corner. The literature considers the Shelling shown in Fig.1d (Nielsen et al., 1999; Esveld, 2001; Kondo et al., 1996 and Rice et al., 1994) as subsurface; it is a dangerous defect that initially develops slowly, and over time the cracks in this defect may favor transverse defects. This defect correlates with internal and manufacturing defects in both its initiation and its propagation. Finally, Fig.1e exemplifies a defect known as squat, or dark spot due to the darkened appearance on the rail surface caused by cracks and plastic deformation of the railhead top.

In this work is characterized a defect from rolling contact fatigue (RCF) which a priori resembles a squat, found in a rail sample provided by VALE S.A. The applied methodology is based on the literature that the Grupo de Pesquisa em Engenharia de Materiais - GPEMAT has adopted.

2. METODOLOGY

2.1 Rail Chemical and Mechanical properties

The rail used in this work has the TR-68 profile which indicates that it contains approximately 68 Kg/m. It transversal profile is divided into three main parts: Head, web and foot (Fig.2). As the focus of this work is to characterize a RCF defect arising from the wheel-rail contact, only the head have been studied.

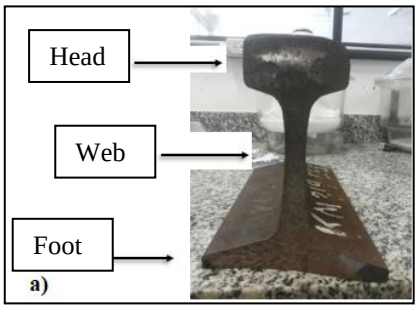

Figure 2. Main rail parts: Head, Web and Foot. Source: From the Survey.

Tensile tests obtained the Ultimate Tensile Strength. Samples were obtained from the head, web, and foot, for this work was considered data only from the railhead.

Surface and transversal hardness measures were obtained using a Rockwell C model 200 HRS-150 durometer, with 1470N load applied and time of 8s as established by ASTM E18-19. For comparison with the literature, the scale conversion of Rockwell C to Brinell was used.

Microhardness measurements were performed in the transversal section using an HV-1000B microdurometer with 500g load. The chemical composition was obtained using a Bruker ® optical emission spectrometer. Three measures

were performed on railhead, three on the web, and three on foot. The types of equipment used to determine material properties are shown in Fig.3.

Figure 3. a) 200 HRS-150 Durometer, b) HV-1000B Microdurometer and c) Q4 TASMAN Optical emission Spectometer. Source: Prazeres, 2014

2.2 – Samples selection and cut

Fig.4 shows the rail that has the defect to be characterized. The image shows oxidation marks that mask the surface aspect of it. A horizontal cut was made at the top of the railhead at about 10 mm depth to obtain the defect sample to be characterized as outlined in Fig.5a. The sample was washed and dried to remove the oxidized layer. Fig.5b illustrates the cuts in the washed part that were made to obtain longitudinal and transverse cross-sections.

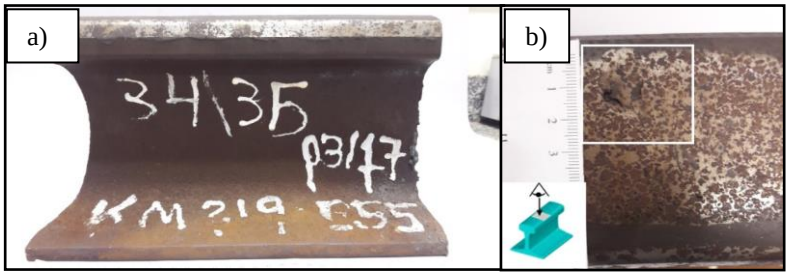

Figure 4. a) Longitudinal cross-section over rail section. b) Top view. The presence of oxidation on the material surface is noteworthy. Source: From the survey.

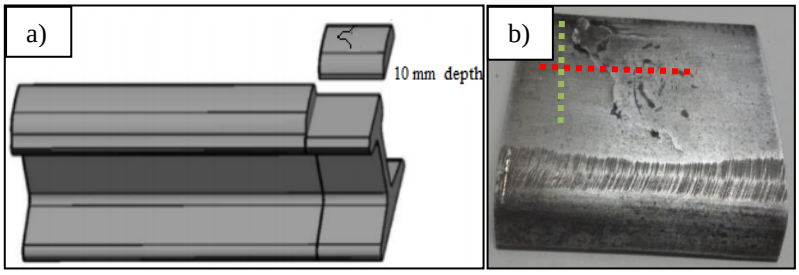

Figure 5. a) Schematic of the sample cut from the top of the rail. Adapted from Al-Juboori, 2019. b) Cutting marks on top. Source: From the survey.

2.3 – Samples preparation

After washing and drying the sample, the surface appearance of the defect can be better observed. The longitudinal and transverse cross-sections were grounded following the standard sequence: 80, 120, 220, 320, 400, 600, 800, 1000, 1200 and 1500 mesh and observed on the stereoscope, first seeking to verify the cracks. Then the samples were polished and etched (Nital 3%) to observe the microstructural behavior using optical microscopy and SEM scanning electron microscopy.

3. RESULTS AND DISCUSSIONS

3.1 Rail Chemical and Mechanical properties

Mechanical properties and chemical composition of the rail material are presented in Tables 1 and 2. The UTS value corresponds only to that obtained from the tensile test in the railhead. Because it contains small amounts of elements

such as Vanadium (V), Nickel (Ni) and Titanium, the rail is classified as microalloyed. Erisir (2012) states that the addition of microalloying elements influences grain refinement and precipitation hardening, obtaining rails with higher mechanical resistance.

Table 1 – Rail mechanical properties. Source: From the survey.

	UTS (MPa)	Superficial hardness (HB)
TR68 rail	1352	390

Table 2 – Rail chemical composition (%W). Source: From the survey.

	C	Mn	Cr	V	P	S	Ni	Ti	Co	Si
TR-68	0.770	0.850	0.415	0.087	<0.005	<0.150	0.032	0.0052	0.023	0.378

The transverse hardness profile of the rail is shown in Fig.6 below. The results are consistent with the literature showing higher values in the head, decreasing towards the foot. This is justified by the fact that the rail is of the head hardened type, having undergone heat treatment.

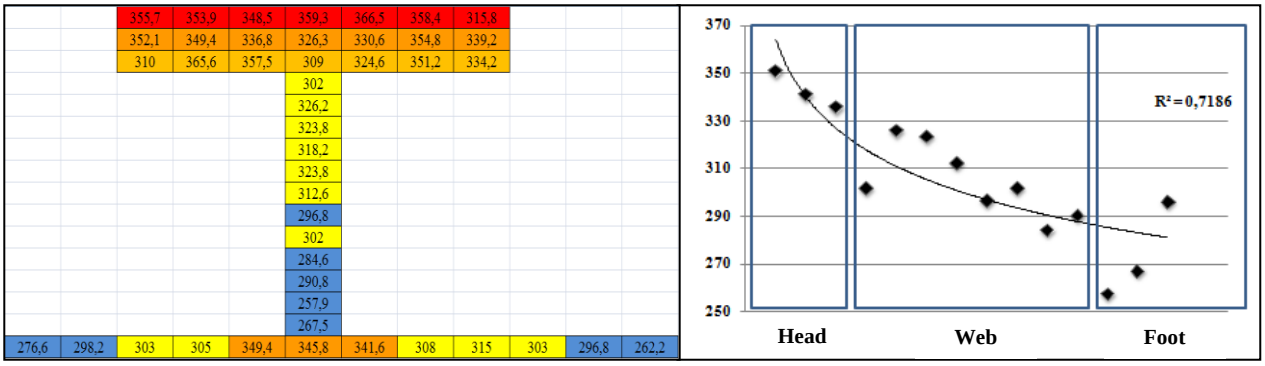

Figure 6 – Rail Brinell hardness transversal profile and graph. Source: From the survey

It is interesting to note that this cross-sectional hardness profile behaves similarly to the residual stress profile on rail subject to service (Fig.7), according to Zerbst (2011). The author comments that at the ends of the foot the residual stress values are lower due to a modified technology during straightening, where the rail goes through a series of rollers. This implies the lower hardness values.

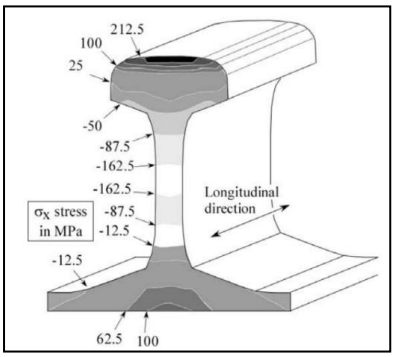

Figure 7 – Longitudinal residual stress components into a serviced rail. Source: Zerbst, 2011.

3.2 Preliminary visual analysis

After the sample was cut and cleaned, the defect was evaluated more accurately. Fig.8 shows this gravity, noticeable the crack that runs through the running surface, being more severe in the region near the field corner (upper Fig.8). Grinding marks are visible in the gauge corner region (bottom of Fig.8).

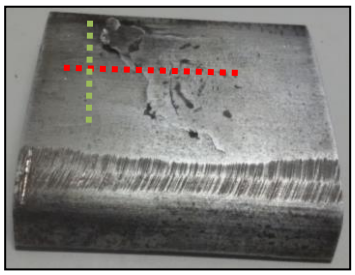

Figure 8. Sample cut and cleaned. Appearance of cracks crossing the full length of the running surface. The dashed red line corresponds to the section in Fig.9 and the dashed green line corresponds to the section in Fig.11. Source: From the survey.

The macrofractography of the longitudinal cross-section (Fig.9) shows the crack propagating subsurface about 0.9 mm deep, then branching until its branches reach about 4.1 mm deep. This crack is dangerous since it propagates in the transverse plane of the rail and its uncontrolled growth can cause the transverse fracture of the component.

Importantly, authors such as Kaewunruen and Ishida (2015) and Deng et al. (2018), investigating the evolution of squats and associating with grinding, in their work showed that the applied grinding removed about 1.0 mm depth of material, which does not guarantee the removal of deeper squats. In this case, this remaining 3.1mm branched crack would continue to grow within the rail.

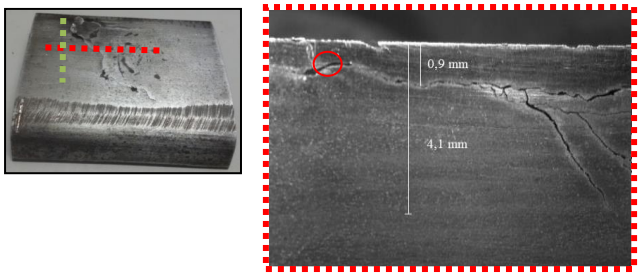

Figure 9. Cracks propagating in subsurface. Magnification: 16x. Source: From the survey.

3.3 - Optical Microscopy

From Fig.10, which represents the 500x magnification of Fig.9 red region, it is possible to see how the microstructure presents heterogeneity close to the crack. This one can be seen in Fig.10b through dark and white effect. At the top is the most aligned microstructure (Region 1), due to ratcheting. The microstructure just below the crack is deformed following the crack propagation direction (region 2). Below is the more dispersed microstructure, justified by the non-interference of the contact (region 3).

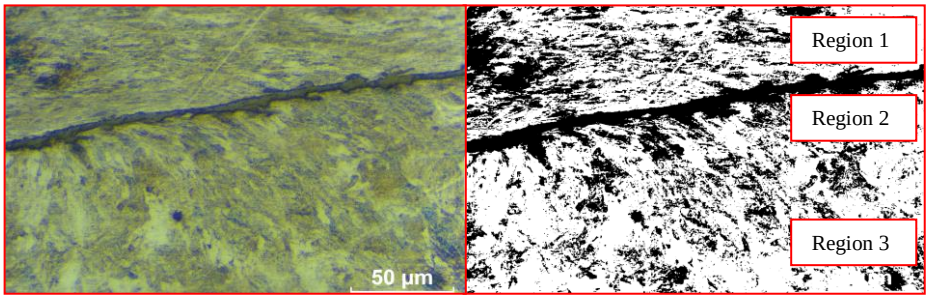

Figure 10. Microstructural aspect of the crack highlighting three distinct regions: Region 1 with perlite lamellas alignment caused by loading, region 2 with the cracks aligned in the direction of crack propagation and region 3 without visible deformation. 500x magnification. Source: from the survey.

It was observed in the field corner through transverse cross-section an isolated crack propagating in the subsurface. Comparing with the literature, this crack is associated with the head check defect. It starts at the edge and penetrates the material until it branches (Fig.11).

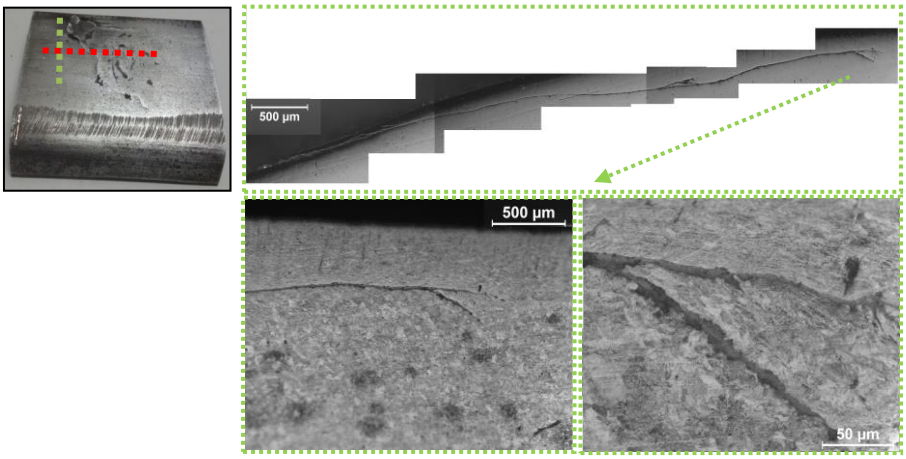

Figure 11. Crack propagation and magnification in or near the crack tip region. Magnification: 200x and 500x. Source: From the survey.

3.4 - SEM

In order to observe the defect using SEM, the sample was washed and cleaned ultrasonically. The material above the defect (peel) was broken off to check internally (Fig.12b). In the internal surface, several wear marks (peelings) were observed, which are removed from the surface after several loading cycles, as shown in Fig.12c and 12d.

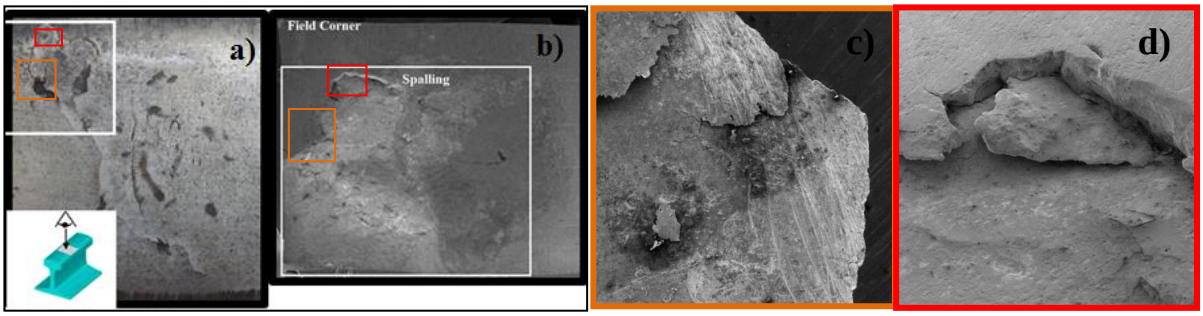

Figure 12. Surface appearance a) before and b) after removal of the upper shell. c) Peelings and d) spalling of material internally to the defect. Magnification: 1200 and 500x Source: From the survey.

The cracks are similar to squat cracks as referred in literature (Steebergen, 2017). There is presence of oxidation associated with fatigue cracks. The literature highlights the influence of fluids (water and oil) entrapped internally in the cracks, which justifies the presence of oxidation (Simon et al, 2012).

The microstructure was confirmed as pearlitic (alternating lamellae of ferrite and cementite). They were obtained in the superficial region about 1.0 mm deep and more internally about 5 mm. Fig.13 shows the difference in orientation of the lamellae, where, when approaching the surface, the lamellae become more aligned and condensed due to loading, featuring ratcheting onset or eutectoid dissociation and increasing hardness.

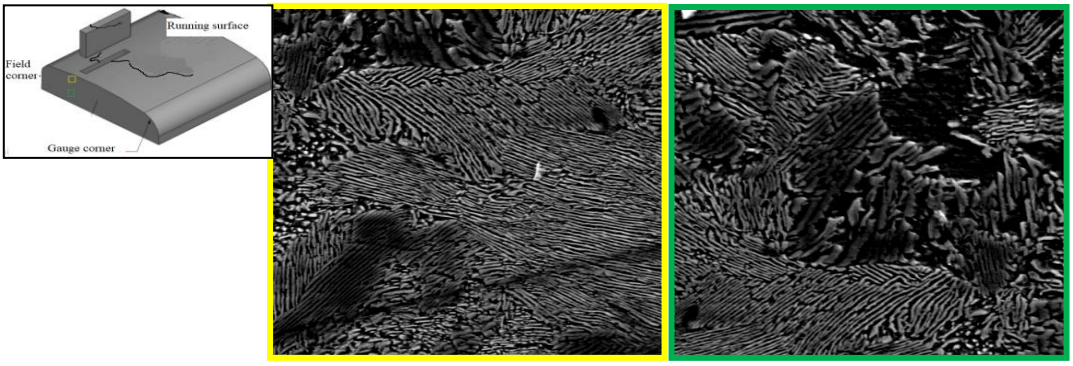

Figure 13. Rail pearlitic microstructure. Magnification: 2700x. Source: From the survey.

3.3 Microhardness Results

The microhardness results in the transverse cross-section allowed us to observe an expected characteristic. Higher microhardness values in the upper rail layers, with values between 390 and 436 HV. High values may be justified by the degree of hardening experienced by the rail surface after several loading cycles. Penetrating more and more into the rail these values decrease until about 5.0 mm deep are found about 350 HV.

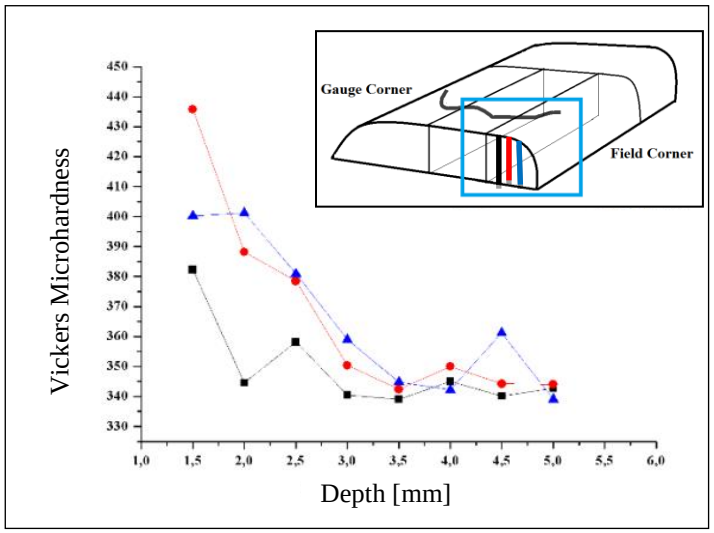

Figure 14. Vickers microhardness of transverse section. Rail hardness may be significantly lower in the lower part of the rail head. Source: From the survey.

4. CONCLUSIONS

Regarding the defect, the conclusions are:

- The mechanical properties and chemical composition correspond to values found in catalogs and steel characterization articles for rails.
- The transverse hardness is consistent, presenting higher values in the railhead because it is heat-treated, intermediate values in the web and lower values in the foot.
- The rail hardness may be significantly lower in the lower part of the rail head. The higher values on the surface are justified by the hardening caused by loading on the rail. Ratcheting was observed, which causes alignment on the perlite lamellae and crack propagation following the direction of this alignment.
- With the naked eye, the defect presents the crack crossing the running surface starting in the field corner region and going towards the corner of the gauge. The longitudinal cross-section showed cracks propagating subsurface and branching to depths of about 4.1 mm.
- The microfractography allowed to observe small peelings within the defect and influenced by many factors, can grow and remove more material from the rail surface.
- A priori, based on the literature, the defect was classified as squat. After analysis of the characteristics, mainly the crack propagation mode, this classification was confirmed.

5. ACKNOWLEDGEMENTS

The authors would like to thank the company VALE SA. by encouraging research through the CÁTEDRA RODA-TRILHO project through FADESP.

6. REFERENCES

American Society for Testing and Materials – *E18- Standard test methods for Rockwell Hardness of metallic materials*. 2019.

Bogdánsky, S; olzak M.; stupinicki, J. *Numerical modelling of a 3d rail rcf 'squat'-type crack under operating load*. Fatigue & Fracture of Engineering Materials & Structures 1998; 21: 923–935

Cannon, DF, Edel K-O, Grassie S, Sawley K. *Rail defects: an overview*. Fatigue Fract Engineering Mater Structure. 2003;26(10):865-887.

Federal railroad administration, *Rolling Contact Fatigue: A Comprehensive Review*, Final report, 2011.

Franklin, F.J. et al. *Modelling rail steel microstructure and its effect on crack initiation*. Wear, v 265, p 1332-1341, 2008.

Garnham, J. E.; Davis, C. L. "*Very early stage rolling contact fatigue crack growt in pearlitic rail steels*" – Wear, v 271, p 100-112, 2011

Grassie, S.L.; Kalousek, J. *Rolling contact fatigue of rails: characteristic, causes and treatment*, in: Proceedings of the 6th International Heavy Haul Association. Conference Proceedings in Cape Town, South Africa, pp. 381–404, 1997

Magel, E. *Rolling contact fatigue: A compreensive review.* Federal Railroad Administration. 2011

Kaewunruen, S.; Ishida, M. *Rail squats: understand its causes, severity, and non-destructive evaluation techniques*. The 20th National Convention on Civil Engineering, 2015.

Deng, X. et al,. *Investigation of the formation of corrugation-induced rail squats based on extensive field monitoring*. International Journal of Fatigue v 112, p 94–105. 2018

He, C.G. et al. *Experimental investigation on the effect of operating speeds on wear and rolling contact fatigue damage of wheel materials*. Wear364-365(2016)257–269

Huang, Y.B. et al. *On the formation and damage mechanism of rolling contact fatigue surface cracks of wheel/rail under the dry condition*. Wear, v 400-401, p 62-73, 2018

Nordco, *Rail Flaw Defects Identification Handbook.* S.n.

Pal, S. et al. *Metallurgical and physical understanding of rail squat initiation and propagation*. Wear, 284-285, p 30-42, 2012.

Simon, S. et al. *Tribological characterization of rail squat defects*. Wear, v 297, p 926-942, 2012.

Steenbergen, M. *Rolling contact fatigue: Spalling versus transverse fracture of rails*. Wear, v 380-381, p 96-105, 2017

Prazeres, E.R. *Estudo do tratamento térmico e da modificação da liga Al0,05%pCu-[0,24-0,28]%pFe-0,6%pMg com a adição de 0,03%pNi*. Trabalho de Conclusão de Curso (TCC). Faculdade de Engenharia Mecânica. Universidade Federal do Pará. 2014.

Popovíc, Z. et al. *The importance of rail inspections in the urban area-aspect of head checking rail defects*. Procedia engineering, v. 117, p. 596-608, 2015.

Zakar, F.; Mueller, E.. *Investigation of a Columbus, Ohio train derailment caused by fractured rail*. Case Studies in Engineering Failure Analysis, v. 7, p. 41-49, 2016.

Australian Rail Track Corporation Ltd, Rail Defects Handbook – *Some Rail defects, their Characteristics, Causes and Control*, 2006.

Stock, R. et al. *Rail grade selection and friction management: a combined approach for optimising rail-wheel contact.* Steelmak. v 40, p 108-114, 2013.

Hardwick, C.; Lewis, R.; Stock, R. *The effect of friction management materials on rail with pre existing RCF surface damage*. Wear, v 384-385, p 50-60, 2017.

2. RESPONSIBILITY NOTICE

The authors are the only responsible for the printed material included in this paper